

Article

# A New Method for the Correction of Spectrum Drift Caused by Temperature Changes When Using a NaI(Tl) Seawater Radioactivity Sensor

Yan Shi, Yingying Zhang \*, Xiandong Feng, Da Yuan, Bingwei Wu and Haijie Bi

Institute of Oceanographic Instrumentation, Qilu University of Technology (Shandong Academy of Sciences), Qingdao 266061, China

\* Correspondence: zhangyysas@163.com

**Abstract:** The seawater radioactivity sensor based on the NaI(Tl) scintillation crystal detection method is prone to spectrum drift due to environment temperature changes during actual measurement, which pose difficulties in the activity analysis of seawater radionuclides. This paper adopts experiment design and analysis methods to study the relationship laws between temperature and peak position channel address and between gain and the peak position channel address. On the basis of studying and summarizing the two relationship laws of the NaI(Tl) seawater radioactivity sensor, a spectrum drift correction method combining gain adjustment and spectrum processing is proposed. Laboratory air and water environment experiments verify that the peak position channel address drift after air environment correction does not exceed  $\pm 2$  channels, and after water environment correction does not exceed  $\pm 1$  channel. Long-term verification experiments at the seawater work site have shown that this correction method can effectively correct the spectrum drift of the NaI(Tl) seawater radioactivity sensor and meet the requirements of long-term automatic operations at sea for the measured spectrum.

**Keywords:** NaI(Tl) seawater radioactivity sensor; spectrum drift; spectrum correction; spectrum processing; seawater radioactivity monitoring



**Citation:** Shi, Y.; Zhang, Y.; Feng, X.; Yuan, D.; Wu, B.; Bi, H. A New Method for the Correction of Spectrum Drift Caused by Temperature Changes When Using a NaI(Tl) Seawater Radioactivity Sensor. *J. Mar. Sci. Eng.* **2024**, *12*, 546. <https://doi.org/10.3390/jmse12040546>

Academic Editor: Christos Tsabaris

Received: 13 November 2023

Revised: 20 December 2023

Accepted: 6 January 2024

Published: 25 March 2024



**Copyright:** © 2024 by the authors. Licensee MDPI, Basel, Switzerland. This article is an open access article distributed under the terms and conditions of the Creative Commons Attribution (CC BY) license (<https://creativecommons.org/licenses/by/4.0/>).

## 1. Introduction

The seawater radioactivity sensor developed based on the NaI(Tl) scintillation crystal detection method has become the main technical means for the in situ automatic monitoring of marine radioactivity environments due to its advantages of programmed, continuous observation. The use of seawater radioactivity sensors for the long-term continuous monitoring of seawater radioactivity levels can provide valuable information for seawater environmental protection [1]. Using full-spectrum analysis technology to analyze the spectrum could achieve the automatic identification and the quantitative detection of multiple radionuclides in seawater [2]. Therefore, the spectrum stabilization performance has become an important topic that provides a guarantee for the validity of measurement data for spectrum analysis.

Seawater temperature changes during the long-term continuous operation of the radioactivity sensor affect the NaI(Tl) scintillation crystal, the photomultiplier, and other electronic components effects [3–5]. Thus, the measured spectrum is affected by environment temperature changes, which add difficulty and even lead to errors for spectrum analysis [6]. Therefore, implementing drift correction on the spectrum obtained from the long-term continuous measurement of the seawater radioactivity sensor is very important.

The current spectrum drift correction methods mainly focus on the radioactivity sensor used in terrestrial environment measurements and can be divided into two categories. The first type is according to the reference peak of the spectrum and achieves spectrum drift correction by adjusting the hardware setting values such as sensor gain [7–9]. The

advantage of this type is that it can correct the large-scale spectrum drift of the seawater radioactivity sensor. The second type reprocesses the measured spectrum using algorithms to obtain the spectrum without drift [10–13]. The advantage of this type is that it does not need to search for peaks during use, and the long-term continuity of the spectrum is good.

Seawater radioactivity sensors are usually deployed on marine-automated monitoring platforms such as buoys for long-term continuous measurement [14]. Based on their working conditions and performance requirements, using only a single type of correction method cannot effectively achieve the spectrum drift correction of the seawater radioactivity sensor. Thus, studying more effective and comprehensive correction methods by combining the two types will achieve better correction results.

This paper conducts temperature experiments on the seawater radioactivity sensor to study and analyze the relationship laws between temperature and peak position channel address and between gain and peak position channel address. The effectiveness and accuracy of the correction method were evaluated through laboratory experiments and verified in the seawater work site by deploying the seawater radioactivity sensor to an offshore platform for long-term measurements.

## 2. Experiment Devices and Methods

### 2.1. Experiment Devices

#### 2.1.1. Seawater Radioactivity Sensor

The seawater radioactivity sensor based on the NaI(Tl) scintillation crystal detection method was used in the experiment (structure is shown in Figure 1), which is mainly composed of the NaI(Tl) scintillation crystal, the photomultiplier, the preamplifier, the digital multichannel pulse amplitude analyzer, the control module, the power module, and the interface module [15]. When the gamma ray in the seawater irradiates the NaI(Tl) scintillation crystal, the crystal emits fluorescence, and the photomultiplier collects the fluorescence and converts it into pulse voltage, which is amplified and shaped before entering the digital multichannel pulse amplitude analyzer for analysis to generate the spectrum. Peaks are generated in the spectrum due to the different counts of a certain channel in multiple channels. Based on the inherent spectrum characteristic peaks of the radionuclides, detailed information on the radionuclides in seawater can be obtained by analyzing the measured spectrum.

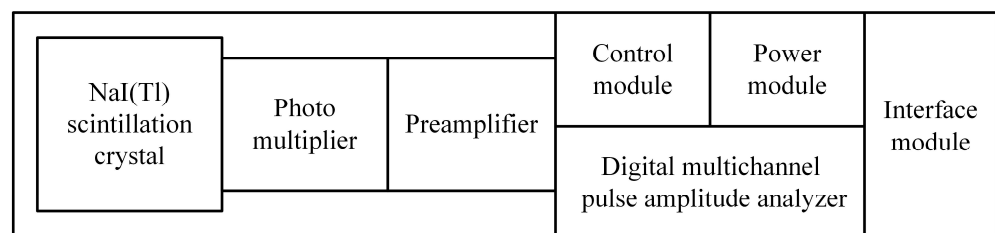


**Figure 1.** Structure of the seawater radioactivity sensor.

The seawater radioactivity sensor is packaged as a whole in a white cylindrical shell, which is waterproof, pressure resistant, and corrosion resistant, ensuring that the seawater radioactivity sensor can work continuously at 200 m underwater. The body of the seawater radioactivity sensor is connected to the shell with a bolt structural joint, and an O-ring is designed at the seal to improve the high tightness of the shell package. The watertight connector provides the seawater radioactivity sensor external power and signal accesses. The measurement condition of minimum detectable activity was the surface seawater off the Chinese coast. The detailed specifications and parameters of the seawater radioactivity sensor are shown in Table 1.

**Table 1.** Specifications and parameters of the seawater radioactivity sensor.

Parameter	Index
Sensor type	3'' × 3'' NaI(Tl)
Energy Range	Adjustable (Max < 3000 keV)
Energy Resolution	<7% (661.6 keV)
Minimum detectable activity	~20 Bq m <sup>-3</sup> (in 24 h) (661.6 keV)
Spectroscopy	1024 channels
Operating temperature	−5~50 °C
Operating voltage	9~18 V DC
Consumption	~2 W
Communication protocol	RS485

### 2.1.2. Temperature Experiment Boxes

Two types of temperature experiment boxes were used in the experiment. The first type was the air temperature experiment box, which has programming operation functions. The air temperature experiment box can control the rate of temperature changes, set the temperature holding time, and adjust the temperature range from −20 °C to 100 °C. Experiments were conducted on the relationship laws between the temperature and the peak position channel address and between the gain and the peak position channel address of the seawater radioactivity sensor in the air temperature experiment box; the two relationship laws were summarized and analyzed, and the spectrum drift correction method was studied. Then, preliminary verification of the correction method was performed in the air temperature experiment box.

The second type was the water temperature experiment box with a temperature adjustment range of −20 °C to 80 °C. Tap water was injected into the box to simulate the working environment of seawater bodies, further verifying the effectiveness and accuracy of the correction method.

## 2.2. Experiment Methods

### 2.2.1. Experiment on the Relationship Law between Temperature and Peak Position Channel Address

Natural radionuclides are ubiquitous in nature, among which the relative contents of <sup>214</sup>Bi, <sup>40</sup>K, and <sup>208</sup>Tl radionuclides are high [16,17], and the three radionuclides can produce more evident natural characteristic peaks in the spectrum. Therefore, when conducting the temperature experiment, three natural characteristic peaks of <sup>214</sup>Bi (609 keV), <sup>40</sup>K (1461 keV), and <sup>208</sup>Tl (2614 keV) were used as references to observe and study the effect of temperature on the spectrum drift.

The temperature range applied in the experiment was the same as the specified working temperature range of the radioactivity sensor: −5 °C to 50 °C. The temperature gradient was 5 °C, and twelve temperature points were set within the temperature range. The temperature of the air temperature experiment box decreased from 50 °C to −5 °C, which is the cooling process, and increased from −5 °C to 50 °C, which is the heating process. Each experiment treated the cooling and heating processes as a measurement cycle to study the drift of the spectrum peak position channel address during different temperature change tendencies and to more accurately investigate the correction method for the spectrum drift.

The experiment of each of the twelve temperature points was performed whenever the temperature in the seawater radioactivity sensor and in the air box controller were equalized for at least 1 h. To obtain a better-quality spectrum, the single spectrum measurement time was 20 min. The drift of the spectrum is the result of the overall temperature effect of all functional modules inside the seawater radioactivity sensor. Therefore, when conducting temperature experiments, the seawater radioactivity sensor must be placed as a whole in the air temperature experiment box (shown in Figure 2).



**Figure 2.** The seawater radioactivity sensor placed as a whole in the air temperature experiment box (left) and the water temperature experiment box (right).

The environment temperature for the energy calibration of the seawater radioactivity sensor used in this paper was 25 °C, so this temperature was the reference temperature point. The measured spectrum under this temperature condition was used as the reference spectrum, and the characteristic peak position channel address was used as the reference peak position channel address.

### 2.2.2. Experiment on the Relationship Law between Gain and Peak Position Channel Address

The  $^{40}\text{K}$  radionuclide relative content in seawater is high [18], and when the seawater environment changes, its relative content remains stable without substantial changes [19]. The seawater radioactivity sensor was completely submerged in seawater during use, and a very noticeable  $^{40}\text{K}$  (1461 keV) natural characteristic peak was formed in the measured spectrum. Therefore, when conducting the gain experiment,  $^{40}\text{K}$  (1461 keV) was used as the characteristic peak for observation and study.

To study the relationship law between gain and the peak position channel address, the air temperature experiment box was used to conduct gain adjustment experiments at different temperatures. Similarly, the temperature change range was  $-5\text{ }^{\circ}\text{C}$  to  $50\text{ }^{\circ}\text{C}$ , the temperature change gradient was  $5\text{ }^{\circ}\text{C}$ , and the reference temperature was  $25\text{ }^{\circ}\text{C}$ . Twelve temperature points were set within the temperature range. The stabilization time to reach each temperature point was greater than 1 h, and the measurement time for each spectrum was 20 min.

When the temperature reached each temperature point, the initial gain was set to 12,000 of the energy calibration. To study the relationship law between gain and peak position channel address accurately and meticulously, the gain was increased or decreased. The gain adjustment gradient was 100, and the gain adjustment range was 9000 to 15,000. Different gain values were used at each temperature point for spectrum measurement to study the influence of gain on peak position channel address.

## 3. Experiment Results and Analysis

### 3.1. Relationship Law between Temperature and Peak Position Channel Address

According to the experiment design of the relationship law between temperature and peak position channel address mentioned earlier, multiple measurement cycle experiments were conducted. Considering the validity and representativeness of the experiment data,

the average peak position channel addresses of  $^{214}\text{Bi}$  (609 keV),  $^{40}\text{K}$  (1461 keV), and  $^{208}\text{Tl}$  (2614 keV) in each temperature point were taken from multiple measurement cycle experiments. Figure 3 shows the relationship of the  $^{214}\text{Bi}$  (609 keV),  $^{40}\text{K}$  (1461 keV), and  $^{208}\text{Tl}$  (2614 keV) peak position channel addresses with the temperature changes.

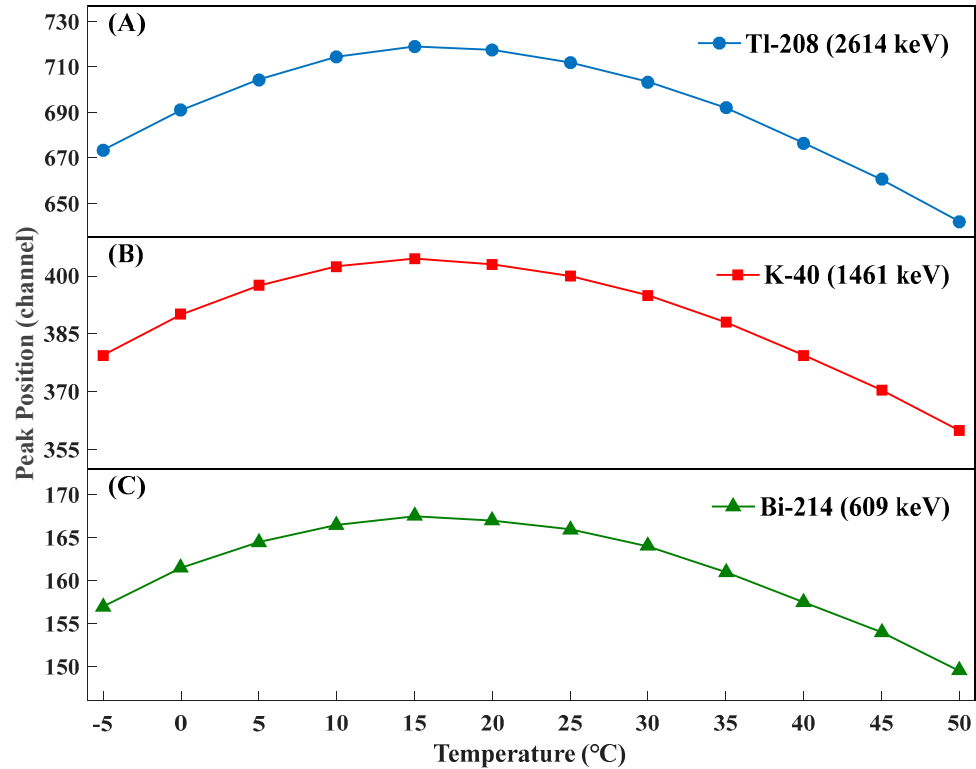


**Figure 3.** Relationship of the peak position channel addresses with the temperature changes for  $^{208}\text{Tl}$  (2614 keV) (A),  $^{40}\text{K}$  (1461 keV) (B), and  $^{214}\text{Bi}$  (609 keV) (C).

Figure 3 shows that the drift of the radionuclide peak position channel address with temperature is not a simple linear relationship. Analysis shows that, within the temperature range of  $-5\text{ }^{\circ}\text{C}$  to  $50\text{ }^{\circ}\text{C}$ ,  $15\text{ }^{\circ}\text{C}$  is the inflection point of the peak position channel address with temperature changes. That is, before  $15\text{ }^{\circ}\text{C}$ , the peak position channel address increases with the increase of temperature, and after  $15\text{ }^{\circ}\text{C}$ , the peak position channel address decreases with the increase of temperature. The relationship law range of  $-5\text{ }^{\circ}\text{C}$  to  $50\text{ }^{\circ}\text{C}$  is the same as in Naumenko et al. [20]; after  $20\text{ }^{\circ}\text{C}$ , it follows the same relationship law as the experiment data in Mitra et al. [21]. However, it is different from the linear function relationship law in Hung et al. [22] and Chen et al. [23]. This outcome is related to factors such as hardware selection, processing programs, and the software algorithms of radioactivity sensors and illustrates the complexity of spectrum drift from another perspective.

However, a great similarity exists in the drift of different radionuclide peak position channel addresses. To explore the relationship law between temperature and different radionuclide peak position channel address drifts, the effect of temperature changes on the full-spectrum range was further investigated. Normalization was performed on different temperature points  $^{214}\text{Bi}$  (609 keV),  $^{40}\text{K}$  (1461 keV), and  $^{208}\text{Tl}$  (2614 keV) peak position channel addresses, as shown in Figure 4.

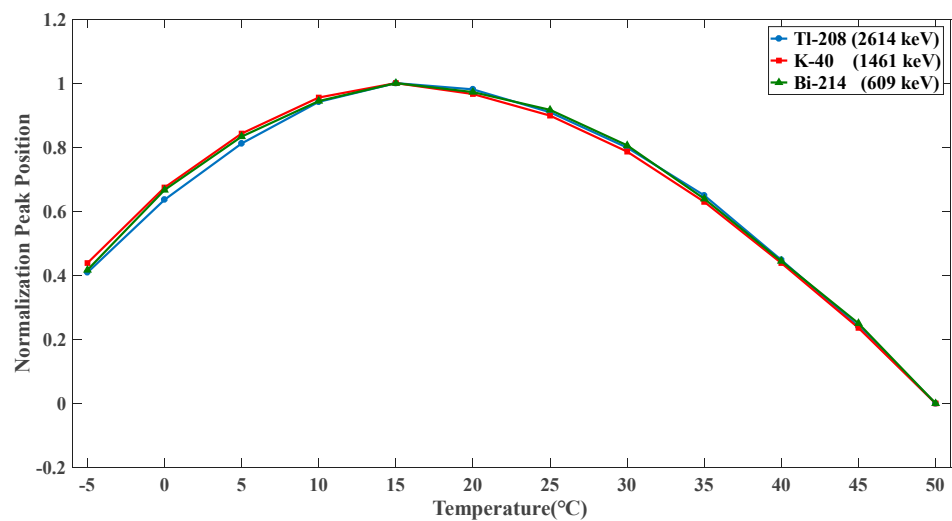


**Figure 4.** Normalization of the peak position channel address.

Figure 4 shows that the normalized peak position channel address of  $^{214}\text{Bi}$  (609 keV),  $^{40}\text{K}$  (1461 keV), and  $^{208}\text{Tl}$  (2614 keV) have the same trend with temperature changes, and the three curves overlap. Therefore, the influence of the same temperature change on different radionuclide peak position channel addresses has the same proportional relationship; that is, if the value of the peak position channel address is large, and the value of the peak position changing with the temperature is large, the change of the spectrum channel address deviation with the temperature is large, and vice versa. This relationship law lays the foundation for establishing a correction method within the full-spectrum range.

Therefore, if the correction relationship between the peak position of a certain characteristic peak in the spectrum is determined, the peak position drift of multiple characteristic peaks and all characteristic peaks within the full-spectrum range can be corrected, thereby correcting all characteristic peaks and the entire spectrum. The theoretical derivation in Casanovas et al. [24] and the experiment data in Bu et al. [25] and Leroux et al. [26] also confirm this view, and this correction relationship is independent of the primary or the quadratic function rule of the peak position channel address drift with temperature.

### 3.2. Relationship Law between Gain and Peak Position Channel Address

According to the experiment design, multiple groups of repeated experiments were conducted at the twelve set temperature points. The multiple groups of  $^{40}\text{K}$  (1461 keV) peak position channel address data at the same temperature point were averaged, and the function relationship between the gain value and the  $^{40}\text{K}$  (1461 keV) peak position channel address was fitted. The results exhibited a good linear function relationship, and the fitting relationship of all temperature points is shown in Table 2. Although the  $^{40}\text{K}$  (1461 keV) peak position corresponds to different channel addresses at varied temperature points, the ratio of the change in the  $^{40}\text{K}$  (1461 keV) peak position channel address with the variation in gain value is approximated, that is, the slope  $k$  value of the fitting relationship is approximated. To simplify the correction method, the  $k$  value at the reference temperature was used as the reference value for the relationship between gain and the peak position channel address.

The fitting relationship between the gain values at the reference temperature point of 25 °C and the  $^{40}\text{K}$  (1461 keV) peak position channel address is shown in Figure 5. A good linear relationship exists between the gain values and the  $^{40}\text{K}$  (1461 keV) peak position channel address (linear correlation coefficient  $R^2 = 0.9999$ ). When the gain value increases, the  $^{40}\text{K}$  (1461 keV) peak position channel address also increases. When the gain value decreases, the  $^{40}\text{K}$  (1461 keV) peak position channel address decreases. The gain has the same influence relationship on the full-spectrum range channel address as the  $^{40}\text{K}$  (1461 keV) peak position channel address due to the consistency of the change ratio and

drift trend of the <sup>214</sup>Bi (609 keV), <sup>40</sup>K (1461 keV), and <sup>208</sup>Tl (2614 keV) peak position channel addresses and the full-spectrum range channel address.

**Table 2.** Fitting relationship between gain values and the <sup>40</sup>K (1461 keV) average peak position channel address at different temperature points.

Temperature Point (°C)	Fitting Relation	R <sup>2</sup>	k
−5	Y = 0.03441X + 13.68	0.9999	0.03441
0	Y = 0.03529X + 14.29	0.9999	0.03529
5	Y = 0.03564X + 15.57	0.9999	0.03564
10	Y = 0.03614X + 14.29	0.9999	0.03614
15	Y = 0.03643X + 14.14	0.9999	0.03643
20	Y = 0.03618X + 16.29	0.9999	0.03618
25	Y = 0.03596X + 15.00	0.9999	0.03596
30	Y = 0.03511X + 20.00	0.9999	0.03511
35	Y = 0.03486X + 14.14	0.9999	0.03486
40	Y = 0.03418X + 14.14	0.9999	0.03418
45	Y = 0.03329X + 13.71	0.9999	0.03329
50	Y = 0.03211X + 16.00	0.9999	0.03211

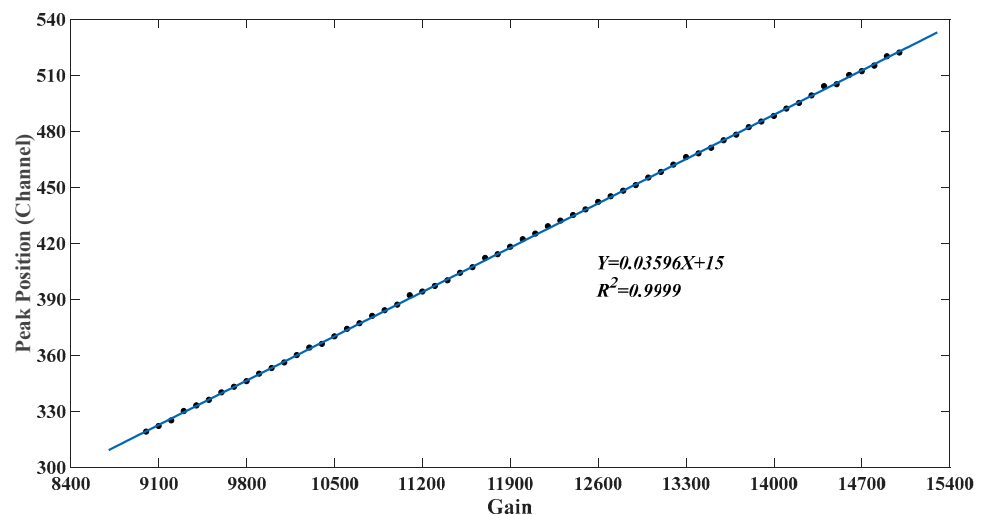


**Figure 5.** Relationship between the gain values and the <sup>40</sup>K (1461 keV) peak position channel address at the reference temperature point.

#### 4. Correction Algorithm and Process

##### 4.1. Correction Algorithm

##### 4.1.1. Gain Adjustment Part Correction Algorithm

The gain adjustment correction part aims to correct the seawater radioactivity sensor to the standard operating state, that is, to eliminate the current spectrum drift state. Using <sup>40</sup>K (1461 keV) as the reference peak for the gain adjustment correction part, when the peak position channel address of <sup>40</sup>K (1461 keV) is corrected to the reference peak position channel address, the spectrum at this time is the reference spectrum, and the working state of the seawater radioactivity sensor is the standard working state.

The deviation of the defined peak position channel address is the difference between the current measured spectrum peak position channel address and the reference peak position channel address:

$$CH_D = PE_S - PE_R \tag{1}$$

where  $CH_D$  is the deviation of the peak position channel address,  $PE_S$  is the peak position channel address of the current measured spectrum, and  $PE_R$  is the reference peak position channel address.

According to the relationship law between the gain and the peak position channel address of the spectrum, the following can be obtained:

$$\frac{GA_D}{CH_D} = \frac{1}{k} \tag{2}$$

where  $GA_D$  represents the gain variation, and  $k$  is the slope of the relationship law between the gain and the peak position channel address.

By combining Equations (1) to (2) and the actual change in gain, the correction formula of the gain adjustment correction part can be obtained:

$$GA_D = -\frac{1}{k} \cdot (PE_S - PE_R) \tag{3}$$

When  $GA_D$  is positive, the current gain should increase. When  $GA_D$  is negative, the current gain should decrease.

The gain adjustment correction part is aimed at quickly and accurately correcting the seawater radioactivity sensor to the standard working state after it is turned on or when it experiences large-scale drift due to abnormal conditions and continuing the spectrum measurement work.

The correction algorithm of the gain adjustment correction part uses the  $^{40}\text{K}$  (1461 keV) natural characteristic peak formed by a large number of  $^{40}\text{K}$  natural radionuclide present in seawater, which solves the problem of introducing the reference source that can have adverse effects on the spectrum of seawater. The correction algorithm is suitable for low-level or extremely low-level radioactivity environments in seawater.

#### 4.1.2. Spectrum Processing Part Correction Algorithm

The previous analysis shows that if the correction relationship of one peak position channel address is determined, then all of the radionuclide characteristic peaks and the full-spectrum range can be effectively corrected. Likewise, the spectrum processing correction part uses the natural characteristic peak of  $^{40}\text{K}$  (1461 keV) to establish a correction algorithm.

The drift of the spectrum channel address with temperature has the same proportion relationship. Therefore, the spectrum with drift can be corrected using the following relationship:

$$CH_{TC} = \frac{CH_T}{F(T)} \tag{4}$$

where  $CH_{TC}$  is the spectrum channel address under a certain temperature condition after correction,  $CH_T$  is the spectrum channel address under a certain temperature condition before correction,  $F(T)$  is the temperature correction function, and  $T$  is the temperature.

The correction function under specific temperature conditions can be expressed as the ratio between the peak position channel address under that temperature condition and the reference peak position channel address:

$$F(T) = \frac{PE_T}{PE_R} \tag{5}$$

where  $PE_T$  is the peak position channel address under a certain temperature condition.

The best fit for the temperature experiment data mentioned above, is a cubic polynomial function:

$$\frac{PE_T}{PE_R} = a + bT + cT^2 + dT^3 \tag{6}$$

where  $a$ ,  $b$ ,  $c$ , and  $d$  are the correction coefficients.

Combining Equations (4) to (6), the correction formula of the spectrum processing correction part is obtained:

$$CH_{TC} = \frac{CH_T}{a + bT + cT^2 + dT^3} \quad (7)$$

In actual work, the environment temperature of seawater usually changes slowly. To ensure that the temperature values used in the spectrum processing correction part are more accurate and representative, the temperature value can be taken as the average of the temperature values from the start, middle, and end of a spectrum measurement period:

$$T_M = \frac{1}{3} \cdot (T_A + T_B + T_C) \quad (8)$$

where  $T_M$  is the average temperature value during the measurement period,  $T_A$  is the temperature value at the start time,  $T_B$  is the temperature value at the middle time, and  $T_C$  is the temperature value at the end time.

By using the correction formula of the spectrum processing correction part, the counts are redistributed on the spectrum channel address, and the peak position channel address, characteristic peak, and spectrum are corrected. Under specific temperature conditions in the laboratory, the quantitative relationship between the temperature and the peak position channel address of the  $^{40}\text{K}$  (1461 keV) natural characteristic peak is obtained. The correction coefficients of the spectrum processing correction part only use the characteristic peak formed by the natural radionuclide, without the need for any radioactivity standard source.

The correction coefficients in the correction algorithm of the spectrum processing correction part are calculated through the quantitative relationship and are only related to the seawater radioactivity sensor itself. After the seawater radioactivity sensor is used in the work site, the spectrum processing correction part does not require any reference peak and only needs to obtain the current temperature value of the measurement environment to correct the spectrum drift, further reducing the complexity of the spectrum analysis.

The seawater radioactivity sensor studied in this paper is based on NaI(Tl) scintillation crystals, which do not possess radioactivity. When using the seawater radioactivity sensor based on LaBr<sub>3</sub>(Ce) or LaCl<sub>3</sub>(Ce) scintillation crystals, the correction coefficients can be calculated using the natural characteristic peaks formed by the scintillation crystals that are self-radioactive [27–29].

#### 4.2. Correction Process

The workflow of the spectrum drift correction method combining gain adjustment and spectrum processing is shown in Figure 6, which can be described as follows: After the seawater radioactivity sensor is turned on, the first step is to perform the gain adjustment correction part, adjust the seawater radioactivity sensor to the standard operating state, and then start measurement according to the sensor settings. During the continuous measurement, every period of the spectrum measurement is completed, and the spectrum processing correction part is performed to obtain the corrected spectrum. The spectrum is automatically saved and accumulated for analysis.

When the conditions of the gain adjustment correction part are reached, the seawater radioactivity sensor automatically performs the gain adjustment correction part according to the settings to correct the seawater radioactivity sensor to the standard operating state and then continues to perform the spectrum measurement and the spectrum processing correction part.

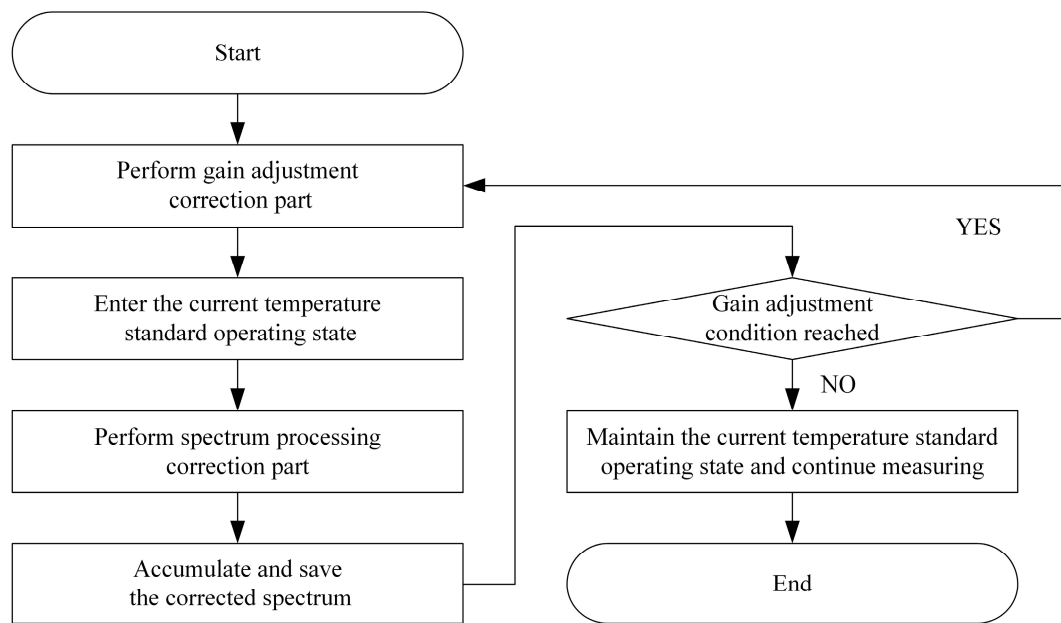


**Figure 6.** Correction method workflow.

If the conditions of the gain adjustment correction part are not reached, the seawater radioactivity sensor does not need to perform the gain adjustment correction part. The measurement is kept in the standard operating state, and the spectrum processing correction part is executed. After the measurement task of the seawater radioactivity sensor is completed, or when the spectrum needs to be extracted, the accumulated and saved spectrum can be used to obtain the corrected long-term spectrum to meet the needs of spectrum analysis.

According to the characteristics of the actual working environment of the seawater radioactivity sensor, when the seawater radioactivity sensor runs in situ for a long-term, the conditions of the gain adjustment correction part can generally be set as follows:

- (1) The cumulative measurement time of the seawater radioactivity sensor exceeds seven days.
- (2) The seawater radioactivity sensor performs the restart operation.
- (3) The seawater radioactivity sensor undergoes considerable changes in the measurement position during use, including displacement changes in the horizontal distance and vertical depth.
- (4) Extreme weather conditions such as strong winds, high waves, and heavy rainfall occur in the deployment sea area of the seawater radioactivity sensor.

## 5. Results and Discussion of Correction Method Verification

### 5.1. Laboratory Verification

#### 5.1.1. Air Environment Correction Method Verification

The air temperature experiment box was used to verify the effectiveness of the proposed correction method preliminarily for the air environment. The experiment steps were the same as the relationship law between the temperature and the peak position channel address, and multiple measurement cycle verification experiments were conducted.

Before using the correction method in the air environment, the typical spectrum drift during the cooling process (Figure 7) and the typical spectrum drift during the heating process (Figure 8) were obtained. After using the correction method in the air environment, the typical spectrum drift during the cooling process (Figure 9) and the typical spectrum drift during the heating process (Figure 10) were acquired.

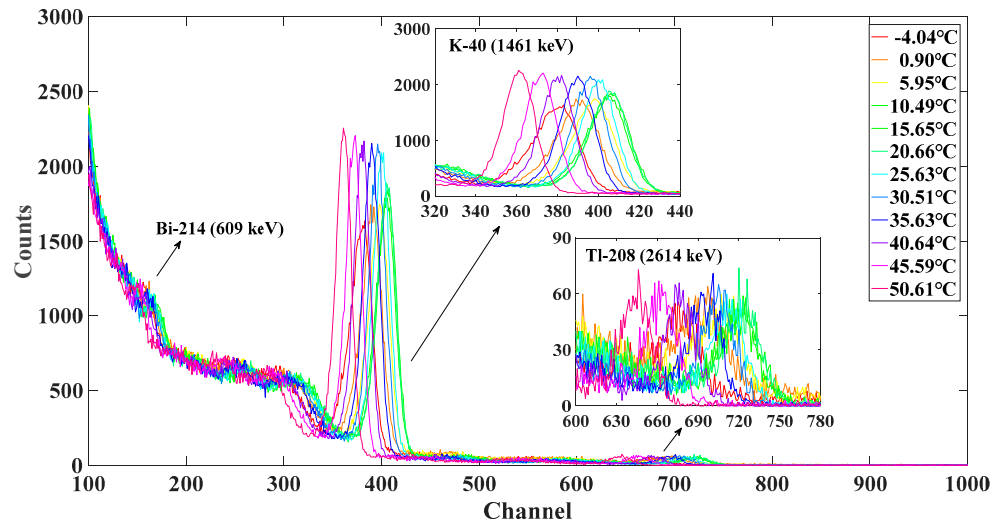


Figure 7. Spectrum drift during the cooling process in the air environment before correction.

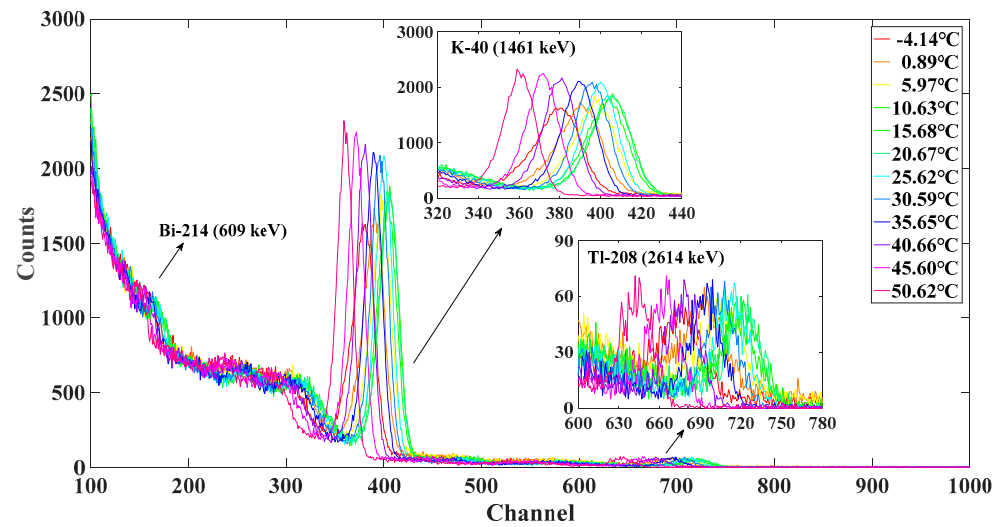


Figure 8. Spectrum drift during the heating process in the air environment before correction.

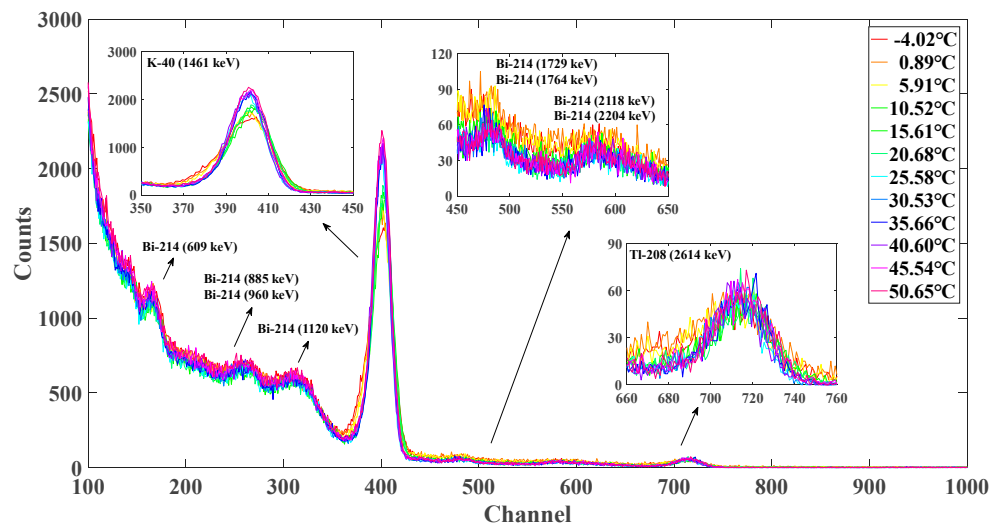
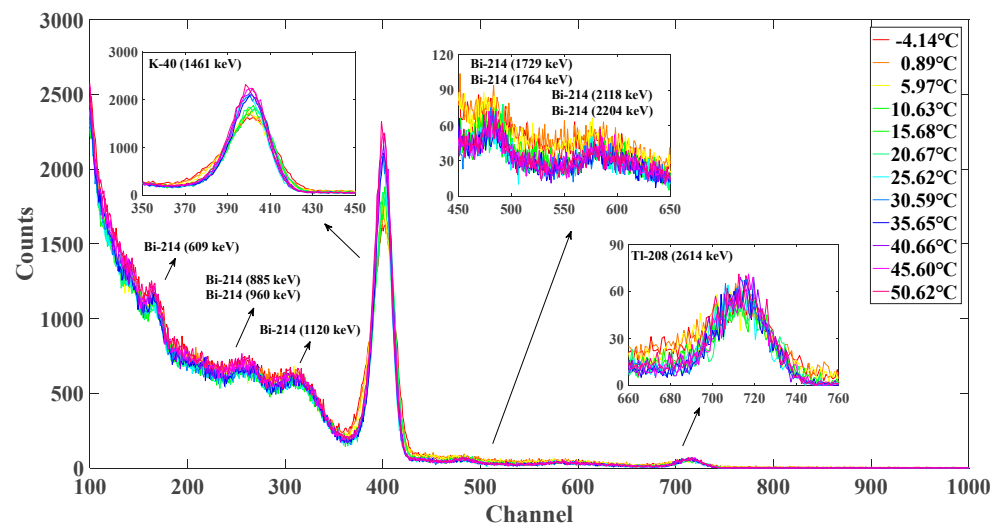


Figure 9. Spectrum drift during the cooling process in the air environment after correction.



**Figure 10.** Spectrum drift during the heating process in the air environment after correction.

Figures 7 and 8 show that before using the correction method, the measured spectrum of each temperature exhibited substantial drift as compared to the reference spectrum, whether during the cooling or heating processes. The amplified  $^{40}\text{K}$  (1461 keV) and  $^{208}\text{Tl}$  (2614 keV) characteristic peaks show that the spectrum with drift has a considerable deviation in the characteristic peak channel address interval, making identifying radionuclides difficult. Meanwhile, interference with the characteristic peak channel address interval of other radionuclides may lead to misjudgment of radionuclide identification, which may adversely affect the analysis of the spectrum. Additionally, during the long-term operation of the seawater radioactivity sensor at sea, the long-term spectrum needs to be synthesized. If the spectrum drifts, it will cause difficulties and reduce the accuracy of the spectrum synthesis and affect the quantitative analysis of various radionuclides in seawater.

At the low-energy  $^{214}\text{Bi}$  (885, 960, and 1120 keV) and middle-energy ends  $^{214}\text{Bi}$  (1729, 1764, 2118, and 2204 keV) of the spectrum, the natural characteristic peaks have fewer counts. Radionuclides cannot be distinguished and identified through the energy calibration formula due to the existence of the spectrum peak position channel address drifts at different temperatures.

Figures 9 and 10 show that after using the correction method, the spectrum drift caused by the temperature changes in the measurement environment during cooling and heating processes is eliminated, and the spectrum measured under different temperature conditions coincide with the reference spectrum. For important channel address intervals in the spectrum analysis, such as the enlarged channel address intervals of  $^{40}\text{K}$  (1461 keV) and  $^{208}\text{Tl}$  (2614 keV) in Figures 9 and 10, the coincidence of the spectrum is good. This result makes the synthesis of long-term measurement more convenient, thereby making the analytical results of long-term continuous automatic measurement spectrum more accurate.

According to the energy calibration formula of the seawater radioactivity sensor, the low-energy end  $^{214}\text{Bi}$  (609, 885, 960, and 1120 keV) and the middle-energy end  $^{214}\text{Bi}$  (1729, 1764, 2118, and 2204 keV) of the spectrum achieve correction for the characteristic peak drift.

To display and analyze the correction results of the spectrum better, Table 3 presents the situation of the  $^{40}\text{K}$  (1461 keV) and  $^{208}\text{Tl}$  (2614 keV) peak position channel addresses with temperature changes after correction. The maximum deviation of the  $^{40}\text{K}$  (1461 keV) peak position channel address does not exceed  $\pm 1$  channel, and the maximum deviation of the  $^{208}\text{Tl}$  (2614 keV) peak position channel address does not exceed  $\pm 2$  channels. The results indicate that the correction method proposed in this paper can effectively correct the peak position channel address of the two target radionuclides,  $^{40}\text{K}$  (1461 keV) and  $^{208}\text{Tl}$  (2614 keV), in the air environment and can effectively correct the drift of the spectrum within the full-spectrum range.

**Table 3.** Comparison of the peak position channel address before and after the use of the correction method in the air environment.

Temperature Point (°C)	Cooling Process				Heating Process			
	Before		After		Before		After	
	<sup>40</sup> K	<sup>208</sup> Tl						
−5	380	675	399	711	379	672	401	711
0	392	695	400	712	392	695	400	712
5	396	705	400	712	397	705	400	712
10	403	717	400	712	403	717	401	712
15	404	718	400	712	405	718	401	712
20	403	717	400	712	403	717	401	712
25	400	712	400	712	399	712	400	712
30	394	701	400	713	394	701	401	713
35	388	690	400	713	388	689	400	713
40	379	676	400	713	379	676	400	713
45	370	660	400	713	370	660	401	714
50	359	641	400	713	360	643	401	714

5.1.2. Water Environment Correction Method Verification

The correction method preliminarily verified through the air environment temperature experiment was written into the seawater radioactivity sensor. To simulate the actual working environment of seawater bodies better when the seawater radioactivity sensor was used, a further design experiment was conducted to verify the correction method in the water environment using the water temperature experiment box. Given the presence of the freezing point of the tap water injected into the water temperature experiment box, the temperature variation range was 0 °C to 50 °C, and other experiment settings and steps were the same as those in the air temperature experiment box. The seawater radioactivity sensor was placed as a whole into the water temperature experiment box (shown in Figure 2), and multiple measurement cycle verification experiments were conducted.

Before using the correction method in the water environment, the typical spectrum drift during the cooling process (Figure 11) and the typical spectrum drift during the heating process (Figure 12) were obtained. After using the correction method in the water environment, the typical spectrum drift during the cooling process (Figure 13) and the typical spectrum drift during the heating process (Figure 14) were obtained.

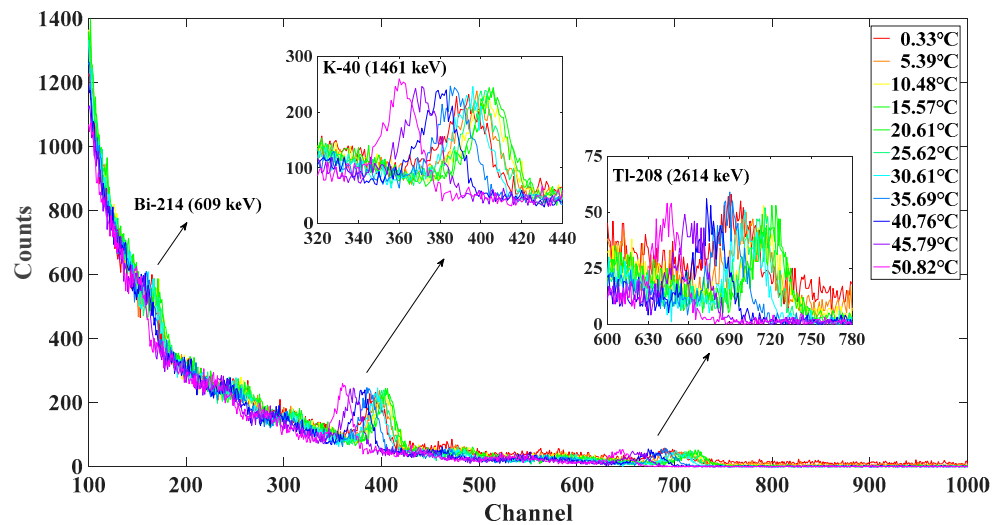


**Figure 11.** Spectrum drift during the cooling process in the water environment before correction.

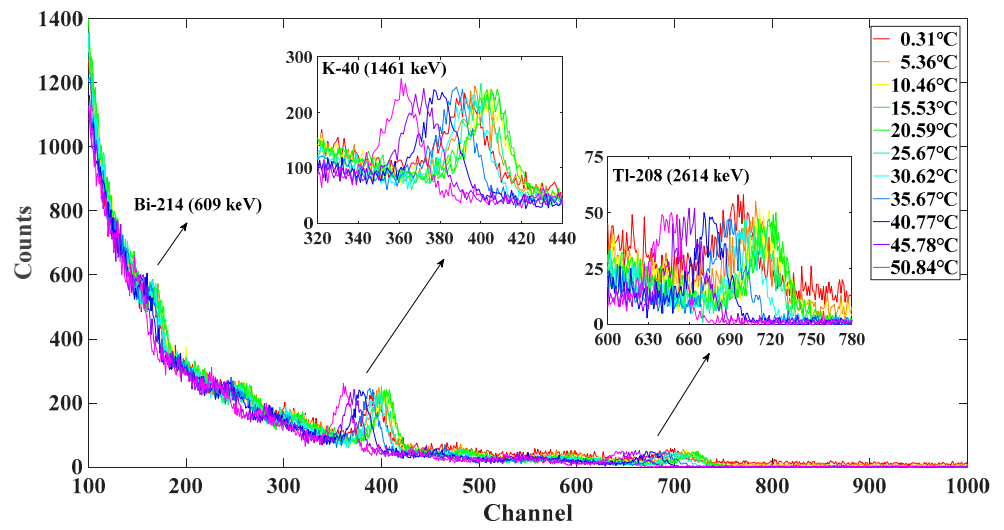


Figure 12. Spectrum drift during the heating process in the water environment before correction.

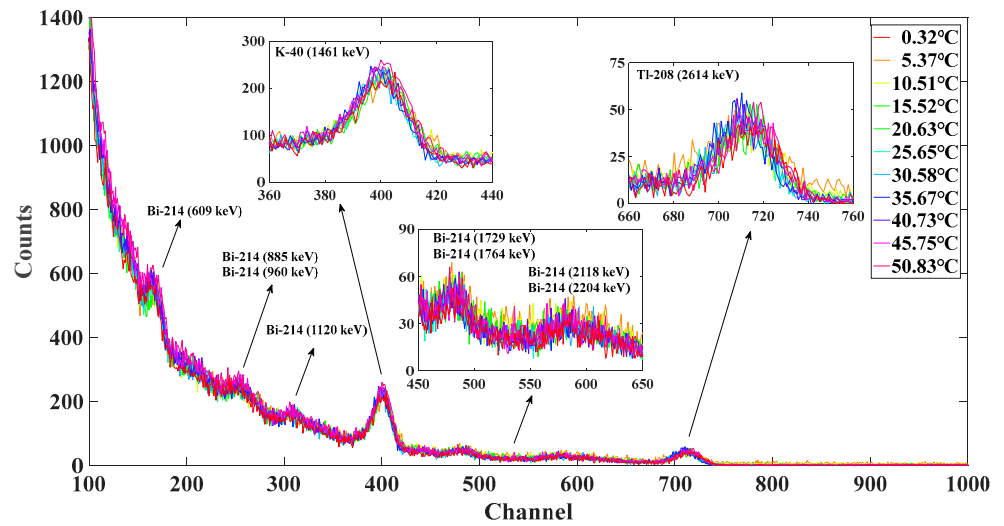


Figure 13. Spectrum drift during the cooling process in the water environment after correction.

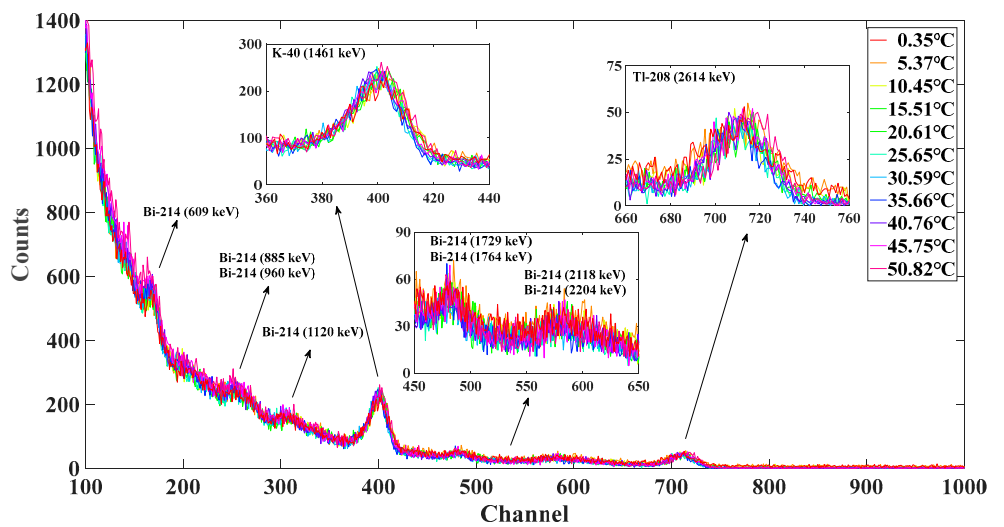


Figure 14. Spectrum drift during the heating process in the water environment after correction.

Figures 11 and 12 show that before using the correction method, the spectrum of the water environment drifts with temperature changes, whether during the cooling or heating processes, and the drift situation is similar to that of the air environment. The reason for the decrease in the spectrum counts in the water environment is the shielding effect of water bodies and the water temperature experiment box on the external radiation environments [30].

Figures 13 and 14 show that during the cooling and heating processes of water environment, due to the automatic implementation of the correction method, the spectrum drift caused by the measurement environment temperature changes in the seawater radioactivity sensor is eliminated. The spectrum measured under different temperature conditions can overlap with the reference temperature spectrum. For important channel address intervals of the spectrum analysis, such as the channel address intervals of the two characteristic peaks  $^{40}\text{K}$  (1461 keV) and  $^{208}\text{Tl}$  (2614 keV), the overlap of the spectrum is good, which is convenient for the synthesis work of the long-term measurement cumulative spectrum, thus making the analysis results of the spectrum obtained from the long-term automatic continuous measurement of the seawater radioactivity sensor more accurate. The  $^{214}\text{Bi}$  (609, 885, 960, and 1120 keV) at the low-energy end and the  $^{214}\text{Bi}$  (1729, 1764, 2118, and 2204 keV) at the middle-energy end of the spectrum achieve characteristic peak drift corrections.

In the verification experiment of the spectrum drift correction method in the water environment, the peak position channel address corresponding to the two characteristic peaks of  $^{40}\text{K}$  (1461 keV) and  $^{208}\text{Tl}$  (2614 keV) in the spectrum measured by the seawater radioactivity sensor are shown in Table 4. The  $^{40}\text{K}$  (1461 keV) peak position channel address completely eliminates drift, and the maximum drift of the  $^{208}\text{Tl}$  (2614 keV) peak position channel address does not exceed  $\pm 1$  channel. The results indicate that the correction method proposed in this paper can effectively correct the peak position channel address of the two target radionuclides  $^{40}\text{K}$  (1461 keV) and  $^{208}\text{Tl}$  (2614 keV) in the water environment and can effectively correct the spectrum drift within the full-spectrum range.

**Table 4.** Comparison of the peak position channel address before and after the use of the correction method in the water environment.

Temperature Point (°C)	Cooling Process				Heating Process			
	Before		After		Before		After	
	$^{40}\text{K}$	$^{208}\text{Tl}$	$^{40}\text{K}$	$^{208}\text{Tl}$	$^{40}\text{K}$	$^{208}\text{Tl}$	$^{40}\text{K}$	$^{208}\text{Tl}$
0	391	694	400	711	391	694	400	711
5	397	706	400	711	398	706	400	711
10	402	716	400	712	402	716	400	711
15	405	719	400	712	405	719	400	712
20	404	718	400	712	404	718	400	712
25	400	712	400	712	400	712	400	712
30	393	700	400	712	393	700	400	712
35	389	691	400	713	389	690	400	712
40	379	677	400	713	379	677	400	713
45	369	659	400	713	369	659	400	713
50	358	640	400	713	359	641	400	713

### 5.2. Seawater Onsite Verification

The seawater radioactivity sensor was deployed to the offshore experiment platform at the Badaxia Wharf (N 36°05', E 120°30') in the Yellow Sea, China. The seawater radioactivity sensor was fixed on a steel frame and sunk into a vertical shaft of the offshore experiment platform (shown in Figure 15). The depth of the vertical shaft was about 5 m, and the seawater radioactivity sensor entered the seawater at a depth of about 3 m, with a depth greater than 2 m from the seabed. This depth considered the effects of cosmic rays and other radioactive environments such as seabed sediments [31–33], making the measurement of the seawater radioactivity environment by the seawater radioactivity sensor more accurate.

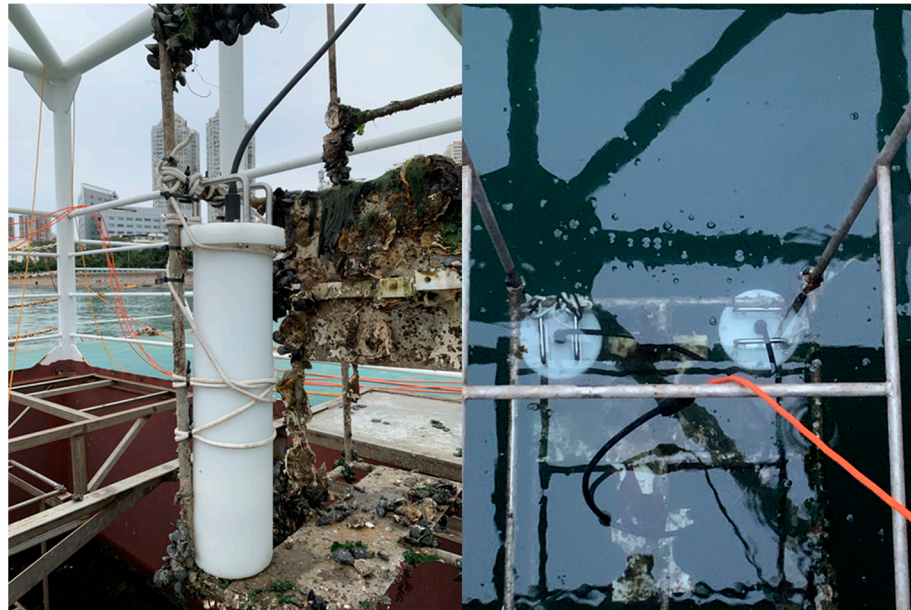


**Figure 15.** Deployment of the seawater radioactivity sensor from the offshore experiment platform.

The reference spectrum was set to the measured spectrum at a temperature of 25 °C, and the reference peak was set to the natural characteristic peak of  $^{40}\text{K}$  (1461 keV) formed by the large number of  $^{40}\text{K}$  radionuclide present in the seawater. The working mode of the seawater radioactivity sensor was set to the continuous automatic measurement mode, with single-spectrum measurement time of 20 min, and the measured seawater spectrum before and after each correction was automatically saved.

On 7 October 2022, the seawater radioactivity sensor was successfully deployed to the offshore experiment platform for the experiment. As of 6 March 2023, the seawater radioactivity sensor had undergone 151 days of continuous experimentation on the offshore experiment platform, successfully obtaining a large amount of seawater spectra. The following section analyzes the measured seawater spectra from two aspects.

#### 5.2.1. Drift Correction under Normal Weather Conditions

Only the characteristic peak of natural radionuclide  $^{40}\text{K}$  (1461 keV) can be clearly observed in the measured seawater spectrum due to the deployment location of the seawater radioactivity sensor, which shields the effects of other radiation environments as much as possible. Therefore, the correction effect analysis was conducted using the characteristic peak of  $^{40}\text{K}$  (1461 keV) as an example. Temperature changes were slower in the seawater environment than in the terrestrial air environment. According to the temperature measurement data, the temperature range of the seawater radioactivity sensor during the entire experiment was 6.03 °C to 21.19 °C. According to the data analysis obtained from the temperature experiments conducted in the laboratory earlier, the drift of the spectrum is not very severe within this temperature range. Taking 24 h as the cumulative time unit of the spectrum, the representative spectrum was selected for analysis. The measured seawater spectrum before correction is shown in Figure 16.

Figure 16 shows the measured seawater spectrum, in late November to early December, had the greater temperature drops registered from 17.29 °C to 10.71 °C. However, the drift of the  $^{40}\text{K}$  (1461 keV) peak position channel address with the temperature is not the most severe. The most severe month of the drift at the  $^{40}\text{K}$  (1461 keV) peak position channel address is from the middle of December to early January, corresponding to the spectra of B, C, D, and E. The reason for this phenomenon is that the drift law of the seawater radioactivity sensor is a quadratic function relationship. Although A and B have large temperature changes, the  $^{40}\text{K}$  (1461 keV) peak position channel address drift is small because A and B are in a slow range of spectrum drift, as is shown in Figure 4 (Section 3.1).

Although the temperature changes of B, C, D, E, and F are small, the drift of the  $^{40}\text{K}$  (1461 keV) peak position channel address is large because B, C, D, E, and F are in the range of intense drift changes in the spectrum.

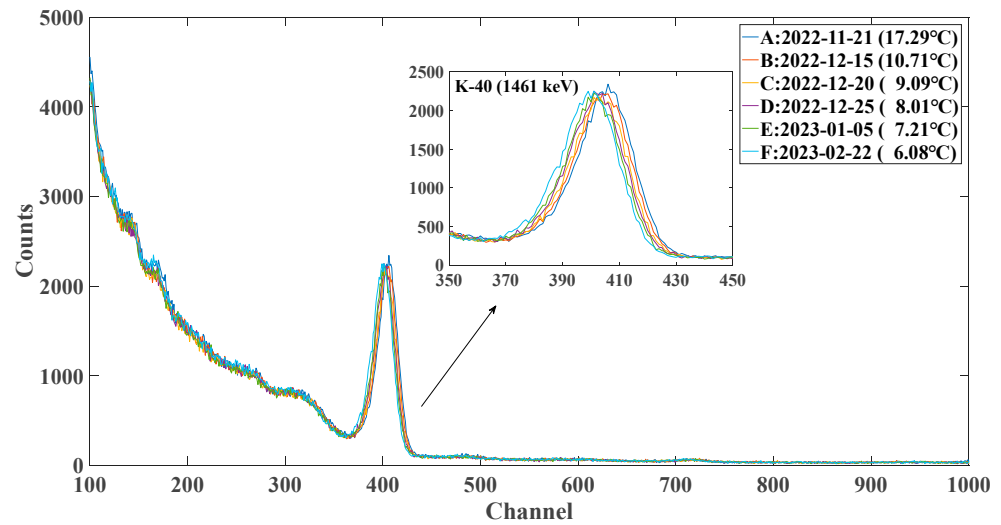


Figure 16. Measured seawater spectrum before correction.

Figure 17 shows the measured seawater spectrum corrected using combined correction methods, corresponding to the seawater gamma spectrum in Figure 16. The  $^{40}\text{K}$  (1461 keV) characteristic peaks of spectra A, B, C, D, E, and F eliminate the drift, and they overlap well. The coincidence of the low-energy end of the spectrum is also better than the uncorrected. With this good foundation, when long-term measured seawater spectra need to be synthesized, the obtained measured seawater spectra will be more accurate, and the resolution of characteristic peak will be better.

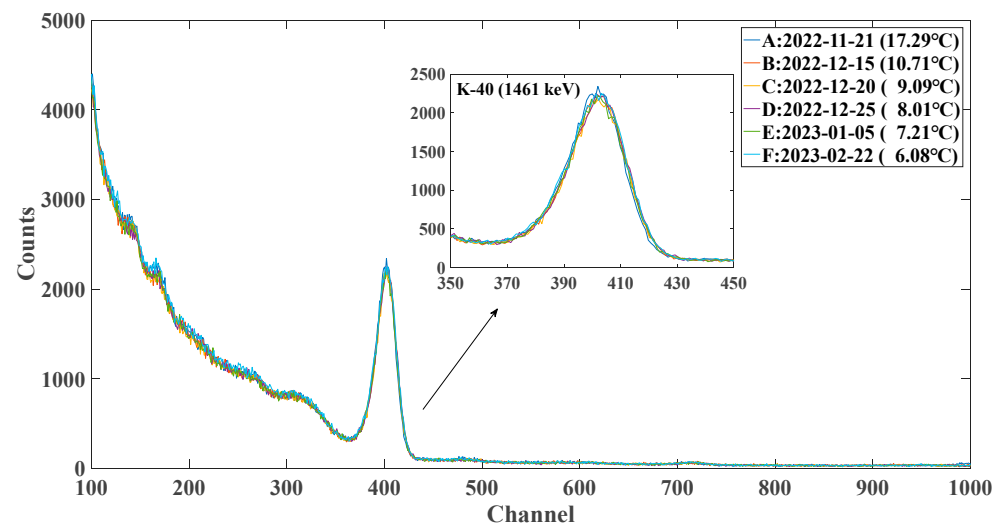


Figure 17. Measured seawater spectrum after correction.

### 5.2.2. Drift Correction under Precipitation Weather Conditions

Precipitation can wash suspended solids of radioactivity in the air and dust can carry radioactive substances from land into seawater [34–37], leading to an increase in the background level of seawater radioactivity [38–40]. Precipitation may also affect the performance of the seawater radioactivity sensor, causing spectrum to drift. During the deployment of the seawater radioactivity sensor to the offshore experiment platform for

the experiment, precipitation monitoring was also carried out, and the two recorded precipitation processes corresponding to the S2 and N2 spectra are shown in Figure 18. When precipitation occurs, the counts of measured seawater spectra substantially increase, and the degree of change is positively correlated with the precipitation. Further analysis shows that the temperatures of S1 and S2, N1 and N2 are almost the same, but due to the influence of precipitation, the peak position channel addresses of  $^{214}\text{Bi}$  (609, 1120, 1729, 1764, 2118, and 2204 keV) undergo substantial drift.

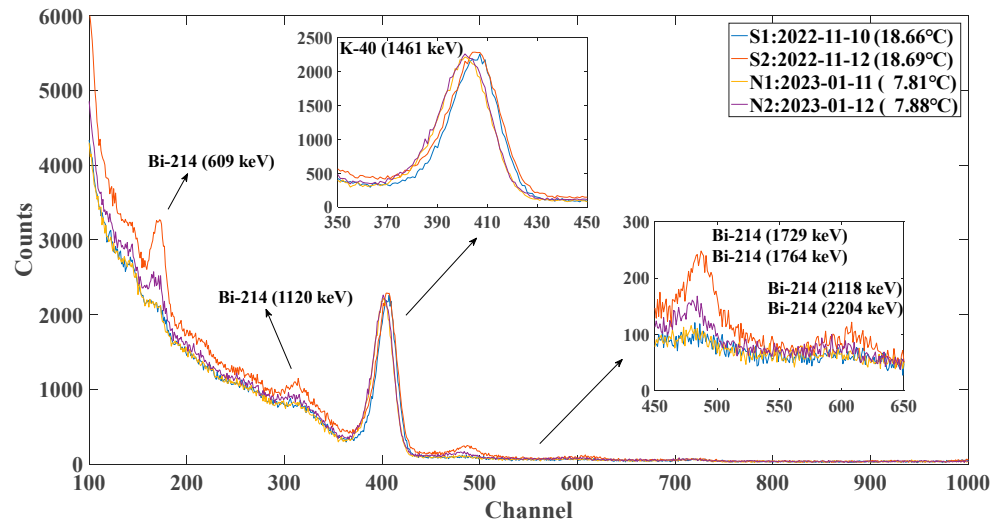


Figure 18. Measured seawater spectrum affected by precipitation before correction.

In Figure 19, S1, S2, N1, and N2, the corrected spectra are obtained by automatically using the correction method, corresponding to the spectra in Figure 18. Whether the  $^{40}\text{K}$  (1461 keV) or the  $^{214}\text{Bi}$  (609, 1120, 1729, 1764, 2118, and 2204 keV) characteristic peak increases due to precipitation, the peak position channel address is automatically corrected back to the position of the reference peak position channel address. Under the same counts, the coincidence of the measured seawater spectrum is also good. This finding indicates that the correction method proposed in this paper can correct the spectrum drift within the full-spectrum range in special working environments such as actual precipitation, and its effectiveness and stability can meet the requirements of practical applications.

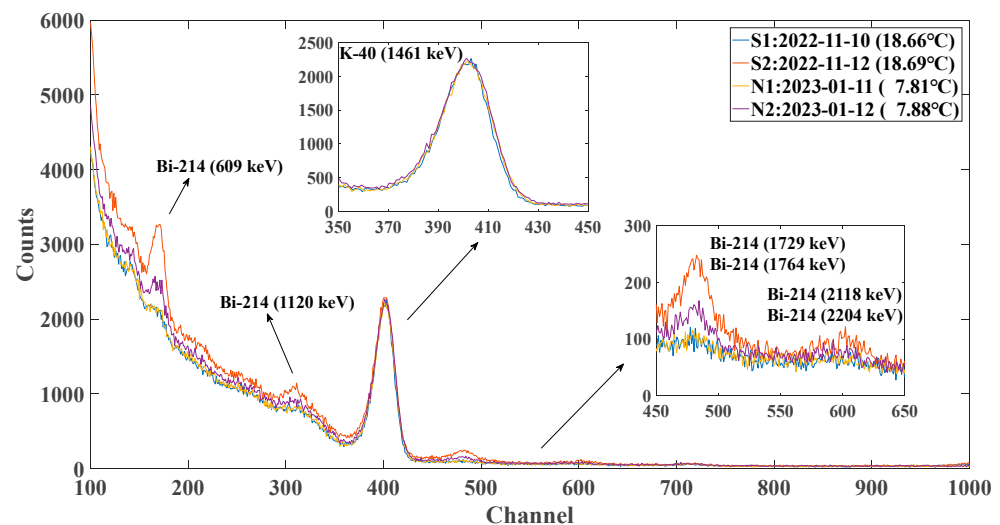


Figure 19. Measured seawater spectrum affected by precipitation after correction.

## 6. Conclusions

This paper studies and discusses the relationship laws between the temperature and peak position channel address and between the gain and the peak position channel address of the NaI(Tl) seawater radioactivity sensor through experiment analysis methods. On this basis, the drift correction method for the NaI(Tl) seawater radioactivity sensor that combines gain adjustment and spectrum processing is proposed. The following main conclusions are drawn:

- (1) When the environment temperature of the seawater radioactivity sensor changes, the peak position channel address is the quadratic function of the temperature, and the inflection point of the peak position channel address change is 15 °C. When the temperature is lower than 15 °C, the peak position channel address increases with the increase of temperature. When the temperature is higher than 15 °C, the peak position channel address decreases with the increase of temperature.
- (2) The drift of different radionuclide characteristic peak positions has the same proportion relationship. The larger the value of the peak position channel address is, the larger the drift amplitude of peak position with the temperature. The smaller the value of the peak position channel address is, the smaller the drift amplitude of the peak position with the temperature.
- (3) The laboratory verification experiment results show that after using the correction method, the coincidence of the spectrum at different temperatures is high, and the maximum number of peak position channel address drifts does not exceed  $\pm 2$  channels. The verification experiment shows that the correction method can effectively correct the drift of the spectrum measured by the seawater radioactivity sensor, and the effectiveness and accuracy of the correction method can meet the drift correction requirements.
- (4) The long-term experiment results of the seawater work site indicate that the correction method can correct the drift of the actual working scene and state of the seawater radioactivity sensor, and the effectiveness and stability of the correction method are very high.

The highlights of the correction method only use a natural characteristic peak of  $^{40}\text{K}$  (1461 keV) without the need for any reference standard sources or modifications to the hardware structure of the seawater radioactivity sensor. Compared with traditional correction methods, the correction method has the advantages of low algorithm complexity and simple flow configuration. The temperature gradients are more evident when the radioactivity sensor operates in the atmospheric environment as compared to the radioactivity sensor operation in the marine environment, and thus this study may play a crucial role for monitoring activities in the atmosphere in order to study air-sea interactions.

**Author Contributions:** Y.S.: Conceptualization, data curation, formal analysis, investigation, methodology, resources, software, validation, visualization, writing—original draft, writing—review and editing; Y.Z.: funding acquisition, project administration, supervision, writing—review and editing; X.F.: investigation, resources, validation; D.Y.: resources, writing—review and editing; B.W.: investigation, resources; H.B.: resources. All authors have read and agreed to the published version of the manuscript.

**Funding:** This work is supported by Taishan Scholar Program, Education and Production Integration Project of Qilu University of Technology (Shandong Academy of Sciences) (No. 2022JBZ01-02-02), Science and Technology Innovation Project of Laoshan Laboratory (No. 2021WHZZB0202; No. LSKJ202204602), Key Research and Development Program of Shandong Province (No. 2023CXPT015), National Key Research and Development Program of China (No. 2023YFC2812900), and National Natural Science Foundation of China (No. U2006222; No. 41606111).

**Data Availability Statement:** Data will be made available on request.

**Conflicts of Interest:** The authors declare no conflicts of interest.

## References

1. Kumar, K.A.; Sundaram, G.A.; Sharma, B.K.; Venkatesh, S.; Thiruvengadathan, R. Advances in gamma radiation detection systems for emergency radiation monitoring. *Nucl. Eng. Technol.* **2020**, *52*, 2151–2161. [\[CrossRef\]](#)
2. Androulakaki, E.G.; Kokkoris, M.; Tsabaris, C.; Eleftheriou, G.; Patiris, D.L.; Pappa, F.K.; Vlastou, R. In Situ  $\gamma$ -ray spectrometry in the marine environment using full spectrum analysis for natural radionuclides. *Appl. Radiat. Isot.* **2016**, *114*, 76–86. [\[CrossRef\]](#)
3. Ianakiev, K.D.; Alexandrov, B.S.; Littlewood, P.B.; Browne, M.C. Temperature behavior of NaI(Tl) scintillation detectors. *Nucl. Instrum. Meth. A* **2009**, *607*, 432–438. [\[CrossRef\]](#)
4. Metwally, W.A.; Gardner, R.P. Stabilization of prompt gamma-ray neutron activation analysis (PGNAA) spectra from NaI detectors. *Nucl. Instrum. Meth. A* **2004**, *525*, 518–521. [\[CrossRef\]](#)
5. Moszyński, M.; Nassalski, A.; Kazuch, A.; Szcześniak, T.; Czarnacki, W.; Wolski, D.; Pausch, G.; Stein, J. Temperature dependences of LaBr<sub>3</sub>(Ce), LaCl<sub>3</sub>(Ce) and NaI(Tl) scintillators. *Nucl. Instrum. Meth. A* **2006**, *568*, 739–751. [\[CrossRef\]](#)
6. Tsabaris, C.; Prospathopoulos, A. Automated quantitative analysis of in-situ NaI measured spectra in the marine environment using a wavelet-based smoothing technique. *Appl. Radiat. Isot.* **2011**, *69*, 1546–1553. [\[CrossRef\]](#) [\[PubMed\]](#)
7. Vlachos, D.S. Self-calibration techniques of underwater gamma ray spectrometers. *J. Environ. Radioact.* **2005**, *82*, 21–32. [\[CrossRef\]](#)
8. Saucke, K.; Pausch, G.; Stein, J.; Ortlepp, H.G.; Schotanus, P. Stabilizing scintillation detector systems with pulsed LEDs: A method to derive the LED temperature from pulse height spectra. *IEEE Trans. Nucl. Sci.* **2005**, *52*, 3160–3165. [\[CrossRef\]](#)
9. Schroettner, T.; Kindl, P. Long term comparison of methods to sustain energy calibration in low level gamma-ray spectroscopy and investigation of possible sources for drift. *Appl. Radiat. Isot.* **2010**, *68*, 164–168. [\[CrossRef\]](#)
10. Choi, Y.; Kim, K.J.; Park, K.; Kim, Y. A LaBr<sub>3</sub>(Ce) detector system with a simple spectral shift correction method for applications in harsh environments. *Radiat. Meas.* **2021**, *142*, 106567. [\[CrossRef\]](#)
11. Qiu, M.; Jia, W.; Hei, D.; Sun, A.; Li, J. Digital stabilization algorithm for the gamma spectra of scintillator detectors in PGNAA. *IEEE Trans. Nucl. Sci.* **2022**, *69*, 113–117. [\[CrossRef\]](#)
12. Wang, C.; Zhang, Q.; Sun, Y.; Liu, J.; Zhou, Y.; Zhang, M. A new numerical correction method for gamma spectra based on the system transformation theory of random signals. *Appl. Radiat. Isot.* **2021**, *172*, 109671. [\[CrossRef\]](#) [\[PubMed\]](#)
13. Zeng, G.; Tan, C.; Ge, L.; Zhang, Q.; Gu, Y. Frequency spectrum analysis for spectrum stabilization in airborne gamma-ray spectrometer. *Appl. Radiat. Isot.* **2014**, *85*, 70–76. [\[CrossRef\]](#) [\[PubMed\]](#)
14. Zhang, Y.; Wang, J.; Vorontsov, A.M.; Hou, G.; Nikanorova, M.N.; Wang, H. Using a neural network approach and time series data from an international monitoring station in the yellow sea for modeling marine ecosystems. *Environ. Monit. Assess.* **2014**, *186*, 515–524. [\[CrossRef\]](#) [\[PubMed\]](#)
15. Zhang, Y.; Wu, B.; Liu, D.; Zhang, Y.; Cheng, Y. Development and deployment of an autonomous sensor for the in-situ radioactivity measurement in the marine environment. *Appl. Radiat. Isot.* **2018**, *142*, 181–186. [\[CrossRef\]](#) [\[PubMed\]](#)
16. Datar, G.; Vichare, G.; Selvaraj, C.; Bhaskar, A.; Raghav, A. Causes of the diurnal variation observed in gamma-ray spectrum using NaI(Tl) detector. *J. Atmos. Sol. Terr. Phys.* **2020**, *207*, 105369. [\[CrossRef\]](#)
17. Kumar, K.A.; Sundaram, G.A.; Thiruvengadathan, R. Advances in detection algorithms for radiation monitoring. *J. Environ. Radioact.* **2020**, *217*, 106216. [\[CrossRef\]](#) [\[PubMed\]](#)
18. Wang, J.; Zhang, Y.; Liu, D.; Wu, B.; Zhang, Y.; Jiang, H. Automated spectra analysis of in situ radioactivity measurements in the marine environment using NaI(Tl) detector. *Appl. Radiat. Isot.* **2018**, *141*, 88–94. [\[CrossRef\]](#)
19. Wang, Y.; Zhang, Y.; Wu, N.; Wu, B.; Liu, Y.; Cao, X.; Wang, Q. Monte Carlo simulation of in situ gamma-spectra recorded by NaI(Tl) detector in the marine environment. *J. Ocean. Univ.* **2015**, *14*, 471–474. [\[CrossRef\]](#)
20. Naumenko, A.; Andrukhovich, S.; Kabanov, V.; Kabanau, D.; Kurochkin, Y.; Martsynkevich, B.; Shoukavy, D.; Shpak, P. Autonomous NaI(Tl) gamma-ray spectrometer for in situ underwater measurements. *Nucl. Instrum. Meth. A* **2018**, *908*, 97–109. [\[CrossRef\]](#)
21. Mitra, P.; Roy, S.A.; Verma, A.K.; Pant, A.D.; Prakasha, M.S.; Anilkumar, S.; Vinod Kumar, A. Application of spectrum shifting methodology to restore NaI(Tl)-recorded gamma spectra, shifted due to temperature variations in the environment. *Appl. Radiat. Isot.* **2016**, *107*, 133–137. [\[CrossRef\]](#) [\[PubMed\]](#)
22. Hung, D.T.; Cao, V.H.; Khang, P.D.; Hai, N.X.; Anh, N.N.; Dinh, D.A.; Hao, T.V.N.; Pham, V. Gamma spectrum stabilization for environmental radiation monitoring stations using NaI(Tl) detector. *Radiat. Prot. Dosim.* **2020**, *189*, 48–55. [\[CrossRef\]](#) [\[PubMed\]](#)
23. Chen, Y.; Li, J.; Zhang, Y.; Xiao, W. Gamma spectrum stabilization method based on nonlinear least squares optimization. *Appl. Radiat. Isot.* **2021**, *169*, 109515. [\[CrossRef\]](#) [\[PubMed\]](#)
24. Casanovas, R.; Morant, J.J.; Salvadó, M. Temperature peak-shift correction methods for NaI(Tl) and LaBr<sub>3</sub>(Ce) gamma-ray spectrum stabilisation. *Radiat. Meas.* **2012**, *47*, 588–595. [\[CrossRef\]](#)
25. Bu, M.; Murray, A.S.; Kook, M.; Helsted, L.M.; Buylaert, J.; Thomsen, K.J. Characterisation of scintillator-based gamma spectrometers for determination of sample dose rate in OSL dating applications. *Radiat. Meas.* **2018**, *120*, 253–259. [\[CrossRef\]](#)
26. Leroux, R.R.; Bezuidenhout, J. An automated drift correction method for in situ NaI(Tl)-detectors used in extreme environments. *Appl. Radiat. Isot.* **2022**, *181*, 110069. [\[CrossRef\]](#) [\[PubMed\]](#)
27. Cheng, H.; Sun, B.; Zhu, L.; Li, T.; Li, G.; Li, C.; Wu, X.; Zheng, Y. Intrinsic background radiation of LaBr<sub>3</sub>(Ce) detector via coincidence measurements and simulations. *Nucl. Sci. Tech.* **2020**, *31*, 99. [\[CrossRef\]](#)
28. Milbrath, B.D.; Choate, B.J.; Fast, J.E.; Hensley, W.K.; Kouzes, R.T.; Schweppe, J.E. Comparison of LaBr<sub>3</sub>:Ce and NaI(Tl) scintillators for radio-isotope identification devices. *Nucl. Instrum. Meth. A* **2007**, *572*, 774–784. [\[CrossRef\]](#)

29. Zeng, Z.; Pan, X.; Ma, H.; He, J.; Cang, J.; Zeng, M.; Mi, Y.; Cheng, J. Optimization of an underwater in-situ LaBr<sub>3</sub>:Ce spectrometer with energy self-calibration and efficiency calibration. *Appl. Radiat. Isot.* **2017**, *121*, 101–108. [[CrossRef](#)]
30. Zhang, Y.; Wu, B.; Liu, D.; Lv, H.; Feng, X. Research on minimum detectable activity (MDA) of underwater gamma spectrometer for radioactivity measurement in the marine environment. *Appl. Radiat. Isot.* **2020**, *155*, 108917. [[CrossRef](#)]
31. Osvath, I.; Povinec, P.P. Seabed gamma-ray spectrometry: Applications at IAEA-MEL. *J. Environ. Radioact.* **2001**, *53*, 335–349. [[CrossRef](#)]
32. Tsabaris, C.; Bagatelas, C.; Dakladas, T.; Papadopoulos, C.T.; Vlastou, R.; Chronis, G.T. An autonomous in situ detection system for radioactivity measurements in the marine environment. *Appl. Radiat. Isot.* **2008**, *66*, 1419–1426. [[CrossRef](#)]
33. Zhang, Y.; Li, C.; Liu, D.; Zhang, Y.; Liu, Y. Monte Carlo simulation of a NaI(Tl) detector for in situ radioactivity measurements in the marine environment. *Appl. Radiat. Isot.* **2015**, *98*, 44–48. [[CrossRef](#)]
34. Patiris, D.; Tsabaris, C.; Livanou, K.; Roumelioti, S.K.; Alexakis, S. Atmospheric in situ gamma-ray spectrometry for precipitation investigation. *Acta Geophys.* **2023**, *71*, 2517–2533. [[CrossRef](#)]
35. Casanovas, R.; Morant, J.J.; Salvadó, M. Implementation of gamma-ray spectrometry in two real-time water monitors using NaI(Tl) scintillation detectors. *Appl. Radiat. Isot.* **2013**, *80*, 49–55. [[CrossRef](#)] [[PubMed](#)]
36. Tsabaris, C. Monitoring natural and artificial radioactivity enhancement in the Aegean Sea using floating measuring systems. *Appl. Radiat. Isot.* **2008**, *66*, 1599–1603. [[CrossRef](#)] [[PubMed](#)]
37. Gusev, A.A.; Martin, I.M.; Alves, M.A.; Abreu, A.J. Simulation of the radiation fallout from gamma-ray measurements. *Model. Earth Syst. Environ.* **2015**, *1*, 18. [[CrossRef](#)]
38. Tsabaris, C.; Ballas, D. On line gamma-ray spectrometry at open sea. *Appl. Radiat. Isot.* **2005**, *62*, 83–89. [[CrossRef](#)] [[PubMed](#)]
39. Zhang, W.; Korpach, E.; Berg, R.; Ungar, K. Testing of an automatic outdoor gamma ambient dose-rate surveillance system in Tokyo and its calibration using measured deposition after the Fukushima nuclear accident. *J. Environ. Radioact.* **2013**, *125*, 93–98. [[CrossRef](#)] [[PubMed](#)]
40. Tsabaris, C.; Androulakaki, E.G.; Ballas, D.; Alexakis, S.; Perivoliotis, L.; Iona, A. Radioactivity monitoring at north Aegean Sea integrating in-situ sensor in an ocean observing platform. *J. Mar. Sci. Eng.* **2021**, *9*, 77. [[CrossRef](#)]

**Disclaimer/Publisher’s Note:** The statements, opinions and data contained in all publications are solely those of the individual author(s) and contributor(s) and not of MDPI and/or the editor(s). MDPI and/or the editor(s) disclaim responsibility for any injury to people or property resulting from any ideas, methods, instructions or products referred to in the content.